2021 43rd Annual International Conference of the
IEEE Engineering in Medicine & Biology Society (EMBC)
Oct 31 - Nov 4, 2021. Virtual Conference

Accelerated image reconstruction with separable Hankel regularization in parallel MRI

Xinlin Zhang, Zi Wang, Xi Peng, Qin Xu, Di Guo, Xiaobo Qu*

Abstract— **Magnetic resonance imaging has been widely adopted in clinical diagnose, however, it suffers from relatively long data acquisition time. Sparse sampling with reconstruction can speed up the data acquisition duration. As the state-of-the-art magnetic resonance imaging methods, the structured low rank reconstruction approaches embrace the advantage of holding low reconstruction errors and permit flexible undersampling patterns. However, this type of method demands intensive computations and high memory consumptions, thereby resulting in a lengthy reconstruction time. In this work, we proposed a separable Hankel low rank reconstruction method to explore the low rankness of each row and each column. Furthermore, we utilized the self-consistence and conjugate symmetry property of k-space data. The experimental results demonstrated that the proposed method outperforms the state-of-the-art approaches in terms of lower reconstruction errors and better detail preservation. Besides, the proposed method requires much less computation and memory consumption.**

Clinical Relevance— **Parallel imaging, image reconstruction, Hankel low-rank**

I. Introduction

As a non-invasive and non-radioactive imaging technique, magnetic resonance imaging (MRI) has served as an indispensable and widely used tool in the clinic [1]. However, the relatively slow acquisition speed limits its application. One of the effective ways to alleviate the prolonged data acquisition time is sparse sampling which acquires only a small subset of the k-space data.

Sparse sampling has emerged as an intensive research field in the past decade, thanks to its effectiveness in shortening the acquisition time and the solid theoretical foundation of the compressed sensing technique. In sparse sampling, the undersampled data is reconstructed using proper priors. Two common priors are sparsity and low-rankness. Sparsity methods assume the image to be sparse in transform domains, such as total variations [2], wavelets [3-7], and adaptive sparse transforms [8-12]. Low-rankness methods utilize the linear correlations among dynamic or high-dimensional MRI images [13-16].

Recently, approaches taking advantage of the structured low rankness of MRI data have been shown to provide promising reconstructions with low reconstruction errors. The structured low-rankness was derived from compact k-space support of coil sensitivities [17], the sparsity of the image in transform domain [18-20], or from finite support of the image/smoothness of image phase [21, 22]. Better reconstructions with the lower error were obtained using those methods than the traditional compressed sensing approaches. However, these approaches need to arrange the MRI data into a high-dimensional structured low-rank matrix. This results in high computation demands and large memory consumption, leading to slow reconstruction time.

In this work, we proposed a new strategy aiming to alleviate this problem and meanwhile to provide better reconstructions. A separable low rank (SHLR) reconstruction method was proposed by enforcing the low rankness of each row and each column of MRI data, avoiding constructing the high-dimensional low-rank matrix thereby enables much less memory cost and allows faster computation. In addition, the self-consistence and conjugate symmetric of k-space data are considered in the proposed formulation. The proposed method permits effective utilization of the low-rank property as the structured low rank does. The experimental results show that the proposed method yield reconstruction with low error and fast speed.

The rest of this paper is organized as follows. Section II presents the proposed model and numerical algorithm, and Section III demonstrates the reconstruction performance. The conclusions are finally drawn in Section IV.

II. Proposed Method

The STDLR-SPIRiT [20] explored the simultaneous horizontal and vertical directional low-rankness in the k-space data, therefore, reduce the image reconstruction errors and outperforms the other state-of-the-art structured low-rank methods. However, the size of the block Hankel matrix appears dramatically huge, leading to a long computational time and large memory requirements.

In this work, instead of constructing a huge size block Hankel matrix, we proposed a separable Hankel low rank reconstruction method to enforce the low-rankness of each row and each column of image as follows:

*Research supported in part by the National Key R&D Program of China (2017YFC0108703), National Natural Science Foundation of China (61971361, 61871341, 61811530021, and U1632274), Health Education Joint Project of Fujian Province (2019-WJ-31), Xiamen University Nanqiang Outstanding Talents Program and China Mobile Communications Group Fujian Co., Ltd. Xiamen Branch Project (XDHT2021004C).
(*Corresponding author: Xiaobo Qu with e-mail: quxiaobo@xmu.edu.cn).

Xinlin Zhang, Zi Wang, and Xiaobo Qu are with the Biomedical Intelligent Cloud R&D Center, Department of Electronic Science, National Institute for Data Science in Health and Medicine, Xiamen University, Xiamen 361105, China.

Xi Peng is with Department of Radiology, Mayo Clinic, Rochester, MN 55902, United States.

Qin Xu are with Neusoft Medical System, Shanghai 200241, China.

Di Guo is with School of Computer and Information Engineering, Xiamen University of Technology, Xiamen 361024, China.

$$\min_{\mathbf{X}} \sum_{m=1}^{M} \left\| \tilde{\mathbf{H}}_{\mathrm{vc}} \tilde{\mathbf{W}} \tilde{\mathbf{F}}^{1\mathrm{D}} \mathbf{P}_m \mathbf{X} \right\|_* + \sum_{n=1}^{N} \left\| \tilde{\mathbf{H}}_{\mathrm{vc}} \tilde{\mathbf{W}} \tilde{\mathbf{F}}^{1\mathrm{D}} \mathbf{Q}_n \mathbf{X} \right\|_* + \frac{\lambda}{2} \left\| \mathbf{Y} - \mathbf{U}\mathbf{F}^{2\mathrm{D}} \mathbf{X} \right\|_F^2 + \frac{\lambda_1}{2} \left\| \mathbf{X} - \mathbf{G}\mathbf{X} \right\|_F^2, \tag{1}$$

where $\mathbf{X} = [\mathbf{X}_1, \mathbf{X}_2, \cdots, \mathbf{X}_J]$ denotes the desired multi-coil image, $\mathbf{X}_j \in \mathbb{C}^{M \times N}$ is the image of the j-th coil, M, N, and J are the number of the row, column, and coil of the data. $\mathbf{F}^{2\mathrm{D}}$ is the 2D Fourier transform for each coil data. The $\mathbf{P}_m$ and $\mathbf{Q}_n$ denote the operators that extract m-th row and n-th column from each coil data for $m = 1, \cdots, M$ and $n = 1, \cdots, N$. Here, we define $\mathbf{x}_{m,j}^{\mathrm{row}}$ as the m-th row of $\mathbf{X}_j$, and $\mathbf{x}_{n,j}^{\mathrm{col}}$ as the n-th column of $\mathbf{X}_j$. With these notations, we have $\mathbf{P}_m \mathbf{X} = \left[\mathbf{x}_{m,1}^{\mathrm{row}}, \cdots, \mathbf{x}_{m,j}^{\mathrm{row}}, \cdots, \mathbf{x}_{m,J}^{\mathrm{row}} \right] \in \mathbb{C}^{N \times J}$ and $\mathbf{Q}_n \mathbf{X} = \left[\mathbf{x}_{n,1}^{\mathrm{col}}, \cdots, \mathbf{x}_{n,j}^{\mathrm{col}}, \cdots, \mathbf{x}_{n,J}^{\mathrm{col}} \right] \in \mathbb{C}^{M \times J}$. The operator $\tilde{\mathbf{H}}_{\mathrm{vc}}$ is defined as:

$$\tilde{\mathbf{H}}_{\mathrm{vc}} \tilde{\mathbf{W}} \tilde{\mathbf{F}}^{1\mathrm{D}} \mathbf{P}_m \mathbf{X} = \left[\mathbf{H}\mathbf{W}\mathbf{F}^{1\mathrm{D}} \mathbf{x}_{m,1}^{\mathrm{row}}, \cdots, \mathbf{H}\mathbf{W}\mathbf{F}^{1\mathrm{D}} \mathbf{x}_{m,J}^{\mathrm{row}}, \mathbf{H}\mathbf{W} \left(\mathbf{F}^{1\mathrm{D}} \mathbf{x}_{m,1}^{\mathrm{row}} \right)^{\dagger}, \cdots, \mathbf{H}\mathbf{W} \left(\mathbf{F}^{1\mathrm{D}} \mathbf{x}_{m,J}^{\mathrm{row}} \right)^{\dagger} \right],$$

$$\tilde{\mathbf{H}}_{\mathrm{vc}} \tilde{\mathbf{W}} \tilde{\mathbf{F}}^{1\mathrm{D}} \mathbf{Q}_n \mathbf{X} = \left[\mathbf{H}\mathbf{W}\mathbf{F}^{1\mathrm{D}} \mathbf{x}_{n,1}^{\mathrm{col}}, \cdots, \mathbf{H}\mathbf{W}\mathbf{F}^{1\mathrm{D}} \mathbf{x}_{n,J}^{\mathrm{col}}, \mathbf{H}\mathbf{W} \left(\mathbf{F}^{1\mathrm{D}} \mathbf{x}_{n,1}^{\mathrm{col}} \right)^{\dagger}, \cdots, \mathbf{H}\mathbf{W} \left(\mathbf{F}^{1\mathrm{D}} \mathbf{x}_{n,J}^{\mathrm{col}} \right)^{\dagger} \right].$$

where the operator $\mathbf{F}^{1\mathrm{D}}$ denotes the 1D Fourier transform on a vector, $\mathbf{W}$ performs weighting on a vector with the weights obtained from applying Fourier transform to 1D sparse transform filter, and $\mathbf{H}$ converts a vector into a Hankel matrix. The tilde above the operator means that the corresponding operation is performed on each column vector of the matrix. The superscript † represents the operation of taking the conjugate and flipping the vector along the center.

The numerical algorithm will be derived to solve the proposed model in Eq. (1) as below. The whole algorithm is summarized in **Pseudo Code**.

TABLE I. THE PSEUDO CODE OF THE ALGORITHM FOR THE PROPOSED SHLR.

Pseudo Code MRI image reconstruction with SHLR.
Input: $\mathbf{Y}$, $\mathbf{U}$, $\mathbf{G}$, λ, λ_1, β, τ.
Initialization: $\mathbf{Z}_m^{\mathrm{row}} = \mathbf{Z}_n^{\mathrm{col}} = \mathbf{0}$, $\mathbf{D}_m^{\mathrm{row}} = \mathbf{D}_n^{\mathrm{col}} = \mathbf{1}$, and $k = 1$.
Output: $\mathbf{X}$.
1: **while** $k < 50$ and $\left\| \mathbf{X}^{(k+1)} - \mathbf{X}^{(k)} \right\|_F^2 / \left\| \mathbf{X}^{(k)} \right\|_F^2 \geq 10^{-6}$ **do**
2: Update $\mathbf{X}^{(k+1)}$ by solving equation (4);
3: Update $\mathbf{Z}_m^{\mathrm{row}(k+1)}$ and $\mathbf{Z}_n^{\mathrm{col}(k+1)}$ by using (6);
4: Update multiplier $\mathbf{D}_m^{\mathrm{row}(k+1)}$ and $\mathbf{D}_n^{\mathrm{col}(k+1)}$ by using (7);
5: $k = k + 1$;
6: **end while**

Introducing $\mathbf{Z}_m^{\mathrm{row}} = \tilde{\mathbf{H}}_{\mathrm{vc}} \tilde{\mathbf{W}} \tilde{\mathbf{F}}^{1\mathrm{D}} \mathbf{P}_m \mathbf{X}$, $\mathbf{Z}_n^{\mathrm{col}} = \tilde{\mathbf{H}}_{\mathrm{vc}} \tilde{\mathbf{W}} \tilde{\mathbf{F}}^{1\mathrm{D}} \mathbf{Q}_n \mathbf{X}$, and Lagrange multiplier $\mathbf{D}_m^{\mathrm{row}}$ and $\mathbf{D}_n^{\mathrm{col}}$, the augmented Lagrangian form of Eq. (1) is

$$\begin{aligned} \max_{\mathbf{D}_m^{\mathrm{row}}, \mathbf{D}_n^{\mathrm{col}}} \min_{\mathbf{X}, \mathbf{Z}_m^{\mathrm{row}}, \mathbf{Z}_n^{\mathrm{col}}} & \sum_{m=1}^{M} \left(\left\| \mathbf{Z}_m^{\mathrm{row}} \right\|_* + \left\langle \mathbf{D}_m^{\mathrm{row}}, \tilde{\mathbf{H}}_{\mathrm{vc}} \tilde{\mathbf{W}} \tilde{\mathbf{F}}^{1\mathrm{D}} \mathbf{P}_m \mathbf{X} \right\rangle + \frac{\beta}{2} \left\| \tilde{\mathbf{H}}_{\mathrm{vc}} \tilde{\mathbf{W}} \tilde{\mathbf{F}}^{1\mathrm{D}} \mathbf{P}_m \mathbf{X} - \mathbf{Z}_m^{\mathrm{row}} \right\|_F^2 \right) \\ & + \sum_{n=1}^{N} \left(\left\| \mathbf{Z}_n^{\mathrm{col}} \right\|_* + \left\langle \mathbf{D}_n^{\mathrm{col}}, \tilde{\mathbf{H}}_{\mathrm{vc}} \tilde{\mathbf{W}} \tilde{\mathbf{F}}^{1\mathrm{D}} \mathbf{Q}_n \mathbf{X} \right\rangle + \frac{\beta}{2} \left\| \tilde{\mathbf{H}}_{\mathrm{vc}} \tilde{\mathbf{W}} \tilde{\mathbf{F}}^{1\mathrm{D}} \mathbf{Q}_n \mathbf{X} - \mathbf{Z}_n^{\mathrm{col}} \right\|_F^2 \right) \\ & + \frac{\lambda}{2} \left\| \mathbf{Y} - \mathbf{U}\mathbf{F}^{2\mathrm{D}} \mathbf{X} \right\|_F^2 + \frac{\lambda_1}{2} \left\| \mathbf{X} - \mathbf{G}\mathbf{X} \right\|_F^2, \end{aligned} \tag{2}$$

where $\langle \cdot, \cdot \rangle$ represents the inner product of the matrix, and β the penalty parameter.

The solution of (2) can be obtained by alternatively solving the following three sub-problems:

The first sub-problem is

$$\begin{aligned} \min_{\mathbf{X}} & \sum_{m=1}^{M} \frac{\beta}{2} \left\| \tilde{\mathbf{H}}_{\mathrm{vc}} \tilde{\mathbf{W}} \tilde{\mathbf{F}}^{1\mathrm{D}} \mathbf{P}_m \mathbf{X} - \mathbf{Z}_m^{\mathrm{row}} + \frac{\mathbf{D}_m^{\mathrm{row}}}{\beta} \right\| + \frac{\lambda}{2} \left\| \mathbf{Y} - \mathbf{U}\mathbf{F}^{2\mathrm{D}} \mathbf{X} \right\|_F^2 \\ & + \sum_{n=1}^{N} \frac{\beta}{2} \left\| \tilde{\mathbf{H}}_{\mathrm{vc}} \tilde{\mathbf{W}} \tilde{\mathbf{F}}^{1\mathrm{D}} \mathbf{Q}_n \mathbf{X} - \mathbf{Z}_n^{\mathrm{col}} + \frac{\mathbf{D}_n^{\mathrm{col}}}{\beta} \right\|_F^2 + \frac{\lambda_1}{2} \left\| \mathbf{X} - \mathbf{G}\mathbf{X} \right\|_F^2, \end{aligned} \tag{3}$$

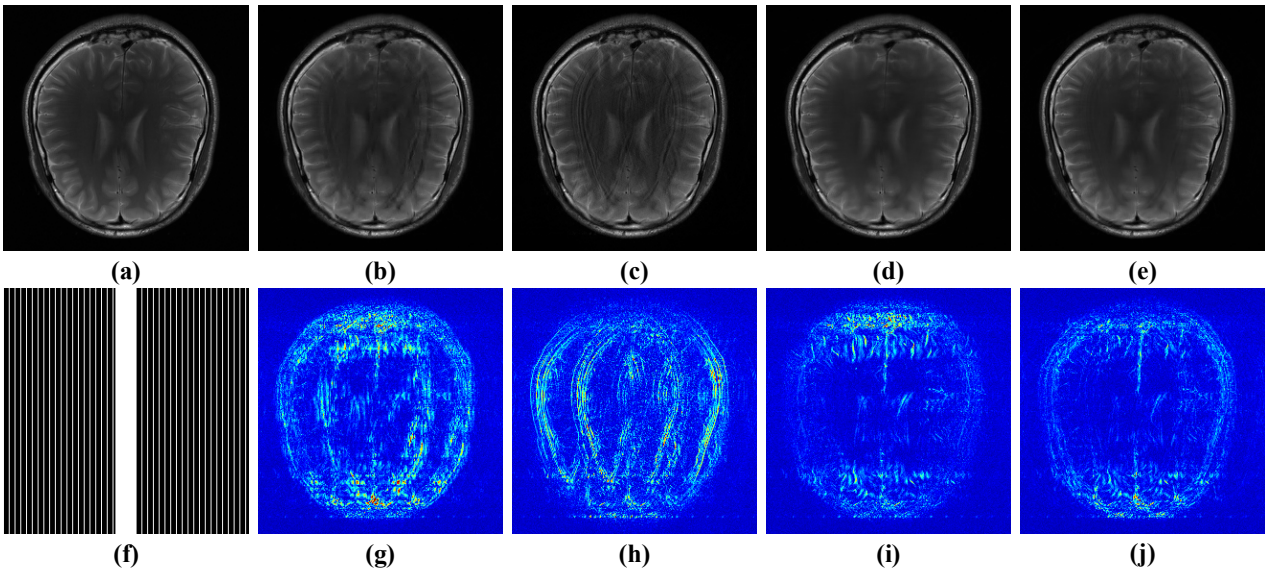

Fig. 1. Reconstruction results and errors under uniform pattern. (a) An SSOS image of fully sampled data; (b-e) SSOS images of reconstructed results by L1-SPIRiT, AC-LORAKS, STDLR-SPIRiT and SHLR-SV, respectively; (f) the uniform undersampling pattern with a sampling rate of 0.23; (g-j) the reconstruction error distribution (10×) corresponding to reconstructed image above them. Note: the RLNE of L1-SPIRiT, AC-LORAKS, STDLR-SPIRiT and SHLR are 0.0935, 0.0936, 0.0714, and 0.0696, respectively.

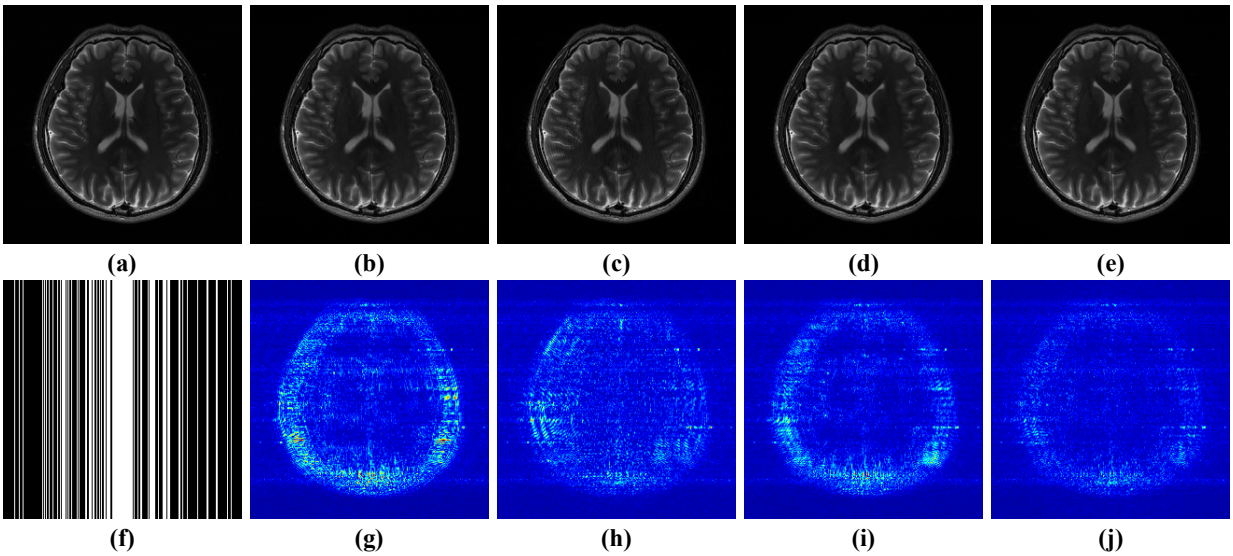

Fig. 2. Reconstruction results and errors under Cartesian pattern. (a) An SSOS image of fully sampled data; (b-e) SSOS images of reconstructed results by L1 -SPIRiT, AC-LORAKS, STDLR-SPIRiT and SHLR, respectively; (f) the Cartesian undersampling pattern with a sampling rate of 0.34; (g-j) the reconstruction error distribution (12.5×) corresponding to reconstructed image above them. Note: the RLNE of L1-SPIRiT, AC-LORAKS, STDLR-SPIRiT and SHLR are 0.0900, 0.0761, 0.0746, and 0.0616, respectively.

whose solution is

$$\begin{aligned}\mathbf{X}=&\left(\lambda\mathbf{F}^{2D,*}\mathbf{U}^{*}\mathbf{U}\mathbf{F}^{2D}+\lambda_1(\mathbf{G}-\mathbf{I})^{*}(\mathbf{G}-\mathbf{I})+\right.\\&\left.\beta\sum_{m=1}^{M}\mathbf{P}_m^{*}\tilde{\mathbf{F}}^{1D,*}\tilde{\mathbf{W}}^{*}\tilde{\mathbf{H}}_{\mathrm{vc}}^{*}\tilde{\mathbf{H}}_{\mathrm{vc}}\tilde{\mathbf{W}}\tilde{\mathbf{F}}^{1D}\mathbf{P}_m+\beta\sum_{n=1}^{N}\mathbf{Q}_n^{*}\tilde{\mathbf{F}}^{1D,*}\tilde{\mathbf{W}}^{*}\tilde{\mathbf{H}}_{\mathrm{vc}}^{*}\tilde{\mathbf{H}}_{\mathrm{vc}}\tilde{\mathbf{W}}\tilde{\mathbf{F}}^{1D}\mathbf{Q}_n\right)^{-1}\times\\&\left(\lambda\mathbf{F}^{2D,*}\mathbf{U}^{*}\mathbf{Y}+\beta\sum_{m=1}^{M}\mathbf{P}_m^{*}\tilde{\mathbf{F}}^{1D,*}\tilde{\mathbf{W}}^{*}\tilde{\mathbf{H}}_{\mathrm{vc}}^{*}\left(\mathbf{Z}_m^{\mathrm{row}}-\frac{\mathbf{D}_m^{\mathrm{row}}}{\beta}\right)+\beta\sum_{n=1}^{N}\mathbf{Q}_n^{*}\tilde{\mathbf{F}}^{1D,*}\tilde{\mathbf{W}}^{*}\tilde{\mathbf{H}}_{\mathrm{vc}}^{*}\left(\mathbf{Z}_n^{\mathrm{col}}-\frac{\mathbf{D}_n^{\mathrm{col}}}{\beta}\right)\right).\end{aligned}\tag{4}$$

The second sub-problem is

$$\begin{aligned}&\min_{\mathbf{Z}_m^{\mathrm{row}}}\left\|\mathbf{Z}_m^{\mathrm{row}}\right\|_{*}+\frac{\beta}{2}\left\|\tilde{\mathbf{H}}_{\mathrm{vc}}\tilde{\mathbf{W}}\tilde{\mathbf{F}}^{1D}\mathbf{P}_m\mathbf{X}-\mathbf{Z}_m^{\mathrm{row}}+\frac{\mathbf{D}_m^{\mathrm{row}}}{\beta}\right\|_F^2,\ m=1,\cdots,M,\\&\min_{\mathbf{Z}_n^{\mathrm{col}}}\left\|\mathbf{Z}_n^{\mathrm{col}}\right\|_{*}+\frac{\beta}{2}\left\|\tilde{\mathbf{H}}_{\mathrm{vc}}\tilde{\mathbf{W}}\tilde{\mathbf{F}}^{1D}\mathbf{Q}_n\mathbf{X}-\mathbf{Z}_n^{\mathrm{col}}+\frac{\mathbf{D}_n^{\mathrm{col}}}{\beta}\right\|_F^2,\ n=1,\cdots,N.\end{aligned}\tag{5}$$

The solution of Eq. (5) lies as

$$\begin{aligned}\mathbf{Z}_m^{\mathrm{row}}&=S_{1/\beta}\left(\tilde{\mathbf{H}}_{\mathrm{vc}}\tilde{\mathbf{W}}\tilde{\mathbf{F}}^{1D}\mathbf{P}_m\mathbf{X}+\frac{\mathbf{D}_m^{\mathrm{row}}}{\beta}\right),\ m=1,\cdots,M\\\mathbf{Z}_n^{\mathrm{col}}&=S_{1/\beta}\left(\tilde{\mathbf{H}}_{\mathrm{vc}}\tilde{\mathbf{W}}\tilde{\mathbf{F}}^{1D}\mathbf{Q}_n\mathbf{X}+\frac{\mathbf{D}_n^{\mathrm{col}}}{\beta}\right),n=1,\cdots,N.\end{aligned}\tag{6}$$

where $S_{1/\beta}(\cdot)$ denotes the soft singular value thresholding operator with the threshold of $1/\beta$ on a matrix.

The third subproblem can be updated by

$$\begin{aligned}\mathbf{D}_m^{\mathrm{row}}&\leftarrow\mathbf{D}_m^{\mathrm{row}}+\tau\left(\tilde{\mathbf{H}}_{\mathrm{vc}}\tilde{\mathbf{W}}\tilde{\mathbf{F}}^{1D}\mathbf{P}_m\mathbf{X}-\mathbf{Z}_m^{\mathrm{row}}\right),\ m=1,\cdots,M,\\\mathbf{D}_n^{\mathrm{col}}&\leftarrow\mathbf{D}_n^{\mathrm{col}}+\tau\left(\tilde{\mathbf{H}}_{\mathrm{vc}}\tilde{\mathbf{W}}\tilde{\mathbf{F}}^{1D}\mathbf{Q}_n\mathbf{X}-\mathbf{Z}_n^{\mathrm{col}}\right),\ n=1,\cdots,N.\end{aligned}\tag{7}$$

III. Results

In this section, we evaluated the performance of the proposed parallel imaging reconstruction method, SHLR, using *in vivo* brain MRI data. The proposed method was compared with three other state-of-the-art reconstruction approaches including L1-SPIRiT [23], AC-LORAKS [22], and STDLR-SPIRiT [20]. The codes of L1-SPIRiT are shared online by Dr. Michael Lustig and codes of AC-LORAKS are shared on Dr. Justin P. Hadard's website. Here, we adopted S-based AC-LORAKS whose formulation make use of phase constraints, since LORAKS with phase constraint provides the best result compared to other constraints [21]. Parameters of all the comparison methods are optimized to obtain the lowest relative L2 norm error (RLNE). Here, the RLNE is defined as

$$\mathrm{RLNE}=\frac{\left\|\mathbf{x}-\hat{\mathbf{x}}\right\|_2}{\left\|\mathbf{x}\right\|_2},\tag{8}$$

where $\mathbf{x}$ and $\hat{\mathbf{x}}$ denotes the column stacked fully sampled k-space data and reconstructed k-space data, respectively. In all experiments, the reconstructed multi-coil images are combined by a square root of the sum of squares (SSOS), and the error distributions of multi coils were combined into a single-coil difference image with SSOS.

Two brain datasets acquired from healthy volunteers are adopted in experiments. The dataset depicted in Fig. 1 (a) is obtained from a 3T SIEMENS Trio MRI scanner (Siemens Healthcare, Erlangen, Germany) equipped with a 32-coil using T2-weighted FLAIR sequence (matrix size = 256 ×256, TR/TE = 3900/9.3 ms, FOV = 200 mm ×200 mm, slice thickness = 5 mm). Eight virtual coils are compressed from the acquired data of 32 coils [24] to reduce the computational complexity. The other dataset shown in Fig. 2 (a) is acquired from a 3T SIEMENS Trio whole-body scanner (Siemens Healthcare, Erlangen, Germany) equipped with a 32-coil using the 2D T2-weighted turbo spin echo sequence (matrix size = 256 ×256, TR/TE = 6100/99 ms, FOV = 220 mm ×220 mm, slice thickness = 3 mm). Four virtual coils are compressed from the acquired data of 32 coils [24]. All computation procedures ran on a CentOS 7 computation server with two Intel Xeon CPUs of 3.5 GHz and 112 GB RAM.

We first validated the proposed method with the 1D uniform undersampling pattern, which is widely adopted in commercial scanners. Both L1-SPIRiT (Fig. 1 (b)) and AC-LORAKS (Fig. 1 (c)) have strong undersampling artifacts.

STDLR-SPIRiT (Fig. 1 (d)) and SHLR (Fig. 1 (e)) show the good ability of artifacts removing. But it is worthy to note that SHLR provides the image with lower error than STDLR-SPIRiT, indicating the excellent ability of the proposed method in terms of artifacts removal and detail preservation.

As shown in Fig. 2, AC-LORAKS (Fig. 2 (c)) yields results exhibiting obvious artifacts inside the internal brain area, whereas the ringing artifacts also remain in the reconstructed image of L1-SPIRiT (Fig. 2 (b)). Both STDLR-SPIRiT (Fig. 2 (d)) and SHLR (Fig. 2 (e)) provide the image with nice artifact suppression. The reconstruction error of STDLR-SPIRiT appears slightly larger than that of SHLR, especially near the skull. The proposed SHLR method permits the relatively lower reconstruction error and edge preservation, appearing robust to the sampling patterns.

The proposed SHLR approach gain a significant reduction in the reconstruction time than STDLR-SPIRiT. The computational time of L1-SPIRiT, AC-LORAKS, STDLR-SPIRiT and the proposed method SHLR are 16.8 seconds, 7.7 seconds, 758.1 seconds, 95.8 seconds, respectively. The running time of SHLR is reduced to 1/8 of that of STDLR-SPIRiT, which dramatically alleviates the burden of lengthy reconstruction time of STDLR-SPIRiT Though the proposed method still runs relatively slower than L1-SPIRiT and AC-LORAKS time runtime of SHLR has been acceptable considering its improvements in the image.

IV. Conclusion

In this paper, we attempted to alleviate huge computational memory consumption of the popular structured low-rank Hankel methods and to improve the reconstructions. Different from the existing structured low-rank Hankel approaches, we did not lift the signal to a very high dimensional Hankel matrix. Instead, we proposed a separable Hankel low rank reconstruction (SHLR) to enforce the low-rankness of each row and each column of the signal of interest. Besides, we imposed the SPIRiT constraint to utilizing the correlation between rows and columns and introduced the conjugate symmetry property into formulation by constructing the Hankel matrix containing the conjugate symmetric. The proposed approach can provide slightly better results with faster reconstruction speed compared to the state-of-the-art methods.

References

[1] J. Hamilton, D. Franson, and N. Seiberlich, "Recent advances in parallel imaging for MRI," *Progress in Nuclear Magnetic Resonance Spectroscopy,* vol. 101, pp. 71-95, 2017.

[2] K. T. Block, M. Uecker, and J. Frahm, "Undersampled radial MRI with multiple coils. Iterative image reconstruction using a total variation constraint," *Magnetic Resonance in Medicine,* vol. 57, no. 6, pp. 1086-1098, 2007.

[3] M. Lustig, D. Donoho, and J. M. Pauly, "Sparse MRI: The application of compressed sensing for rapid MR imaging," *Magnetic Resonance in Medicine,* vol. 58, no. 6, pp. 1182-1195, 2007.

[4] X. Qu, W. Zhang, D. Guo, C. Cai, S. Cai, and Z. Chen, "Iterative thresholding compressed sensing MRI based on contourlet transform," *Inverse Problems in Science and Engineering,* vol. 18, no. 6, pp. 737-758, 2010.

[5] Y. Liu, Z. Zhan, J. Cai, D. Guo, Z. Chen, and X. Qu, "Projected iterative soft-thresholding algorithm for tight frames in compressed sensing magnetic resonance imaging," *IEEE Transactions on Medical Imaging,* vol. 35, no. 9, pp. 2130-2140, 2016.

[6] X. Zhang *et al.*, "A guaranteed convergence analysis for the projected fast iterative soft-thresholding algorithm in parallel MRI," *Medical Image Analysis,* vol. 69, p. 101987, 2021.

[7] Y. Hu *et al.*, "Spatiotemporal flexible sparse reconstruction for rapid dynamic contrast-enhanced MRI," *IEEE Transactions on Biomedical Engineering,* doi: 10.1109/TBME.2021.3091881, 2021.

[8] S. Ravishankar and Y. Bresler, "MR image reconstruction from highly undersampled k-space data by dictionary learning," *IEEE Transactions on Medical Imaging,* vol. 30, no. 5, pp. 1028-1041, 2011.

[9] X. Qu, Y. Hou, F. Lam, D. Guo, J. Zhong, and Z. Chen, "Magnetic resonance image reconstruction from undersampled measurements using a patch-based nonlocal operator," *Medical Image Analysis,* vol. 18, no. 6, pp. 843-856, 2014.

[10] Z. Zhan, J. Cai, D. Guo, Y. Liu, Z. Chen, and X. Qu, "Fast multiclass dictionaries learning with geometrical directions in MRI reconstruction," *IEEE Transactions on Biomedical Engineering,* vol. 63, no. 9, pp. 1850-1861, 2016.

[11] Z. Lai *et al.*, "Image reconstruction of compressed sensing MRI using graph-based redundant wavelet transform," *Medical Image Analysis,* vol. 27, pp. 93-104, 2016.

[12] S. Ravishankar and Y. Bresler, "Data-driven learning of a union of sparsifying transforms model for blind compressed sensing," *IEEE Transactions on Computational Imaging,* vol. 2, no. 3, pp. 294-309, 2016.

[13] Z. Liang, "Spatiotemporal imaging with partially separable funcrions," in *2007 4th IEEE International Symposium on Biomedical Imaging: From Nano to Macro*, 2007, pp. 988-991.

[14] B. Zhao, J. P. Haldar, A. G. Christodoulou, and Z. Liang, "Image reconstruction from highly undersampled (k, t)-space data with joint partial separability and sparsity constraints," *IEEE Transactions on Medical Imaging,* vol. 31, no. 9, pp. 1809-1820, 2012.

[15] R. Otazo, E. Candès, and D. K. Sodickson, "Low-rank plus sparse matrix decomposition for accelerated dynamic MRI with separation of background and dynamic components," *Magnetic Resonance in Medicine,* vol. 73, no. 3, pp. 1125-1136, 2015.

[16] J. Yao, Z. Xu, X. Huang, and J. Huang, "An efficient algorithm for dynamic MRI using low-rank and total variation regularizations," *Medical Image Analysis,* vol. 44, pp. 14-27, 2018.

[17] P. J. Shin *et al.*, "Calibrationless parallel imaging reconstruction based on structured low-rank matrix completion," *Magnetic Resonance in Medicine,* vol. 72, no. 4, pp. 959-970, 2014.

[18] K. Jin, D. Lee, and J. Ye, "A general framework for compressed sensing and parallel MRI using annihilating filter based low-rank Hankel matrix," *IEEE Transactions on Computational Imaging,* vol. 2, no. 4, pp. 480-495, 2016.

[19] G. Ongie and M. Jacob, "Off-the-grid recovery of piecewise constant images from few Fourier samples," *SIAM Journal on Imaging Sciences,* vol. 9, no. 3, pp. 1004-1041, 2016.

[20] X. Zhang *et al.*, "Image reconstruction with low-rankness and self-consistency of k-space data in parallel MRI," *Medical Image Analysis,* vol. 63, p. 101687, 2020.

[21] J. P. Haldar, "Low-rank modeling of local k-space neighborhoods (LORAKS) for constrained MRI," *IEEE Transaction on Medical Imaging,* vol. 33, no. 3, pp. 668-81, 2014.

[22] J. P. Haldar, "Autocalibrated loraks for fast constrained MRI reconstruction," in *2015 IEEE 12th International Symposium on Biomedical Imaging (ISBI)*, 2015, pp. 910-913.

[23] M. Lustig and J. M. Pauly, "SPIRiT: Iterative self-consistent parallel imaging reconstruction from arbitrary " *Magnetic Resonance in Medicine,* vol. 64, no. 2, pp. 457-71, 2010.

[24] D. Bahri, M. Uecker, and M. Lustig, "ESPIRIT-based coil compression for cartesian sampling," in *International Society for Magnetic Resonance in Medicine*, 2013, p. 2657.